Chemical Science

ROYAL SOCIETY OF CHEMISTRY

EDGE ARTICLE

View Article Online
View Journal | View Issue

Cite this: *Chem. Sci.*, 2024, **15**, 19496

All publication charges for this article have been paid for by the Royal Society of Chemistry

Received 27th August 2024
Accepted 31st October 2024

DOI: 10.1039/d4sc05756b

rsc.li/chemical-science

Large second harmonic generation and birefringence from extended octupolar π-conjugated structures†

Danyang Dou, [a] Bingbing Zhang, [ab] Daqing Yang [a] and Ying Wang *[ab]

The exploration of crystal materials for optical manipulation by nonlinear optical (NLO) and anisotropic light–matter interaction is of paramount importance in modern science and technology. However, in such crystal materials, finding the right balance between second harmonic generation (SHG), birefringence, and the bandgap presents a significant challenge. In this contribution, we employ extended octupolar π-conjugated groups devoid of intrinsic dipole moments to construct melonate-based inorganic–organic hybrid crystals, thereby achieving simultaneous large optical nonlinearity and anisotropy. In accordance with this strategy, $Rb_3[C_6N_7(NCN)_3]\cdot 3H_2O$ (I) and $Cs_3[C_6N_7(NCN)_3]\cdot 3H_2O$ (II) were obtained and subjected to detailed investigation. Strong SHG responses of ~9× KH_2PO_4 and a large birefringence of at least 0.6@546 nm were observed for I and II crystals, respectively, together with a suitable bandgap for visible-UV application. Theoretical calculations indicated that octupolar $[C_6N_7(NCN)_3]^{3-}$ groups of I and II arranged in a near parallel configuration exhibit a discrete π electron distribution, resulting in enhanced NLO susceptibilities and maximal polarizability difference. This work underscores the potential of octupolar structures with extended π-conjugation as a promising avenue for the discovery of NLO and birefringence crystals.

Introduction

As an important component of cutting-edge optical materials, nonlinear optical (NLO) and birefringent crystals have plentiful frontier applications in the military, medical, and aerospace fields.[1–5] However, the development of high-performance optical functional crystal materials with strong second-harmonic generation (SHG) and large optical anisotropy continues to face significant challenges.[6–10] High-performance optical materials rely on special functional units with a significant microscopic SHG response and optical anisotropy, and achieve their optimal spatial arrangement within the lattice. The design of non-centrosymmetric (NCS) heteroanionic groups such as $[BO_3F]$,[11] $[SO_3NH_2]$,[12,13] $[PO_3F]$,[14] $[PO_3NH_3]$,[15] $[MoO_2O_4]$,[16] $[SbO_2F_2]$,[17] $[YO_3F_3]$,[18] $[SbO_4F_2]$,[19] and MF_7 (M = Zr, Hf)[20] has been a recent hot topic in the study of NLO and birefringent materials. A common feature of these asymmetric functional units is their large intrinsic dipole moments, which usually lead to strong microscopic NLO polarizability. However, as the dipole functional units usually produce dipole–dipole interactions in the crystal leading to antiparallel arrangements, they eventually form centrosymmetric (CS) materials that are SHG inert. In addition, such antiparallel arrangements also cancel out optical anisotropy, resulting in limited birefringence.[17,21]

Recently, small flat π-conjugated groups have been widely adopted as the basic building units (BBUs) to design optical materials. Borates containing planar π-conjugated $[BO_3]^{3-}$ and $[B_3O_6]^{3-}$ groups have been considered a treasure trove of UV NLO materials,[22] such as the classical NLO materials $KBe_2BO_3F_2$ (KBBF),[23] $Sr_2Be_2B_2O_7$,[24] and β-BaB_2O_4 (BBO).[25] In subsequent studies, a series of cyanurates containing organic planar π-conjugated $[C_3N_3O_3]^{3-}$ groups similar to $[B_3O_6]^{3-}$ have been reported to have excellent linear and nonlinear properties,[26] *e.g.*, $Ca_3(C_3N_3O_3)_2$ (CCY)[27] and β-$Sr_3(C_3N_3O_3)_2$ (β-SCY).[28] Meanwhile, the $Cs_3C_3N_3(NCN)_3\cdot 3H_2O$ crystal containing the triazine $[C_3N_3]$-nuclear derivative $[C_3N_3(NCN)_3]^{3-}$ exhibits a strong SHG response and large birefringence.[29] By extending the π-conjugated system, the derivative of the heptazine $[C_6N_7]$-core, $[C_6N_7O_3]^{3-}$, was also proved to be an excellent high-performance NLO moiety.[30] It is interesting to point out that these π-conjugated anionic groups are octupolar moieties, and are organized into a two-dimensional (2D) layered structure that exhibits a strong SHG and significant birefringence.[17,31,32]

[a]*College of Chemistry and Materials Science, Key Laboratory of Medicinal Chemistry and Molecular Diagnosis of the Ministry of Education, Hebei Research Center of the Basic Discipline of Synthetic Chemistry, Key Laboratory of Chemical Biology of Hebei Province, Hebei University, Baoding 071002, China. E-mail: wangy@hbu.edu.cn*

[b]*Institute of Life Science and Green Development, Hebei University, Baoding 071002, China*

† Electronic supplementary information (ESI) available: Crystallographic data, PXRD, additional crystal pictures, EDX results, XPS, IR spectra, TG-DSC curves, UV-vis-NIR diffuse reflectance spectra, and theoretical calculations. CCDC 2375217 and 2375218. For ESI and crystallographic data in CIF or other electronic format see DOI: https://doi.org/10.1039/d4sc05756b

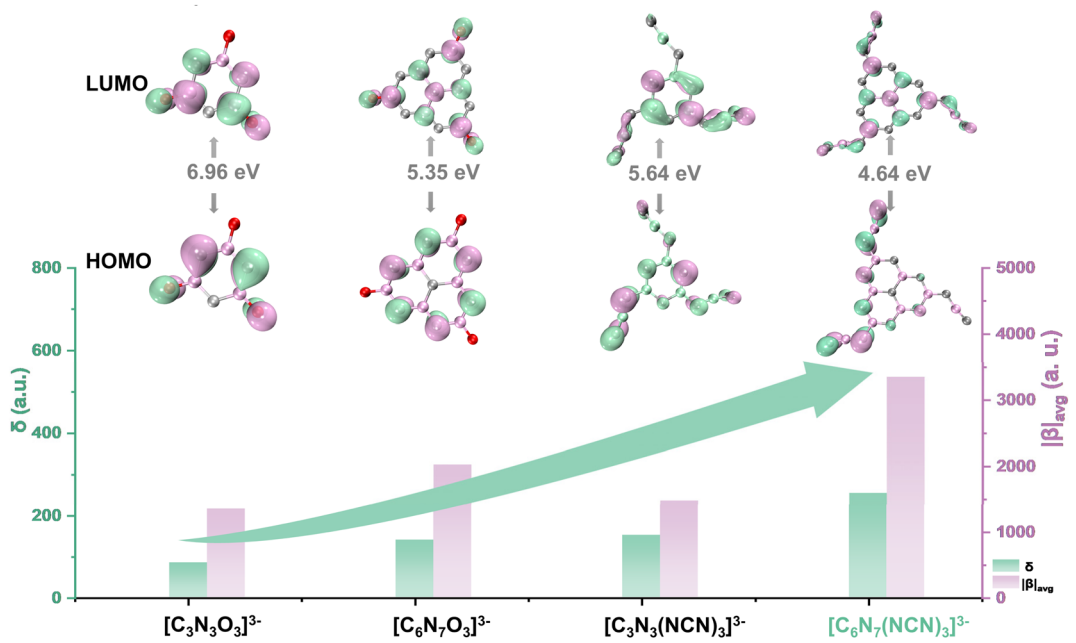

Fig. 1 The comparison of $|\beta|_{avg}$, δ, and E_g for diverse octupolar π-conjugated structures.

Nevertheless, achieving a balanced trade-off among SHG, birefringence and the bandgap remains a significant challenge, with considerable scope for further optimization.

Here, we proposed an idea to create high-performance optical materials by extending the octupolar π-conjugated system. This perspective is informed by the following considerations: (1) octupolar structures that are frequently encountered in C_3 or S_4 point groups (or subgroup) are eventually NCS structures without an intrinsic dipole moment.[33] Therefore, they can retain a favorable NCS spacing arrangement without unwanted dipole–dipole interactions in the crystal, leading to a large SHG.[34–37] (2) The higher degree of π electron delocalization helps enhance the NLO and birefringent properties.[26] (3) Given that a colossal π-conjugated system would result in a reduction of the bandgap, an extended or discrete π-conjugated system could be a viable alternative for achieving balanced comprehensive properties.[38] To verify this strategy, we compared the calculated average first-order hyperpolarizability ($|\beta|_{avg}$), polarizability anisotropy (δ), and energy gap (E_g) between the highest occupied molecular orbitals (HOMOs) and the lowest unoccupied molecular orbitals (LUMOs) for diverse octupolar π-conjugated structures including $[C_3N_3O_3]^{3-}$, $[C_6N_7O_3]^{3-}$, $[C_3N_3(NCN)_3]^{3-}$, and $[C_6N_7(NCN)_3]^{3-}$ (Fig. 1). It is known that $|\beta|_{avg}$, δ, and E_g are important parameters for reflecting the bulk SHG, birefringence, and bandgap, respectively. It was found that $|\beta|_{avg}$ and δ increase significantly as the number of π-conjugation atoms increases, while reduction of E_g is acceptable.

To evaluate the π-bonding properties of the above octupolar π-conjugated structures, the localized orbital locator integrated over the π plane (LOL-π)[39] has been plotted using the Multiwfn code[40] (Fig. 2 and S1†). The visualization reveals a favorable delocalization path of π electrons. It is clear that π electron populations on the cyanurate and heptazine core show delocalization features, while a more localized π electron distribution within C≡N bonds is observed in the side arms of $[C_3N_3(NCN)_3]^{3-}$ and $[C_6N_7(NCN)_3]^{3-}$ groups. The electron localization function over the π plane (ELF-π) isosurface analyses[39] further identify the degree of π electron delocalization of these systems. Unlike $[C_3N_3O_3]^{3-}$ and $[C_6N_7O_3]^{3-}$, there are two adjacent ELF-π domains in $[C_3N_3(NCN)_3]^{3-}$ or $[C_6N_7(NCN)_3]^{3-}$ as the isovalue increases to 0.6. Owing to the linear (N–C≡N) side arms, the π electron distribution in the latter two cases are discrete, which could help increase the induced polarizability while retaining the relatively large E_g. Compared with other octupolar π-conjugated structures, $[C_6N_7(NCN)_3]^{3-}$ shows the largest discrete π electron distribution, leading to more dispersed electron density over the whole anion, and eventually reached higher NLO susceptibilities, larger optical anisotropy and suitable HOMO–LUMO gaps.

By adopting the above strategy, we prepared two excellent optical functional materials, $Rb_3[C_6N_7(NCN)_3]\cdot 3H_2O$ (**I**) and $Cs_3[C_6N_7(NCN)_3]\cdot 3H_2O$ (**II**). Interestingly, **I** and **II** not only demonstrate a strong SHG response (~1.5× BBO) but also exhibit substantial birefringence (~0.6@546 nm), which stand out among other nonlinear and linear optical materials. This work points out a new strategy to construct high performance optical crystals for nonlinear and anisotropic optical application.

Results and discussion

Single crystals of **I** and **II** were grown from water solution by slow solvent evaporation and the antisolvent diffusion method, respectively (see the Experimental section in the ESI†). We provide alternative synthesis routes for melonate salts

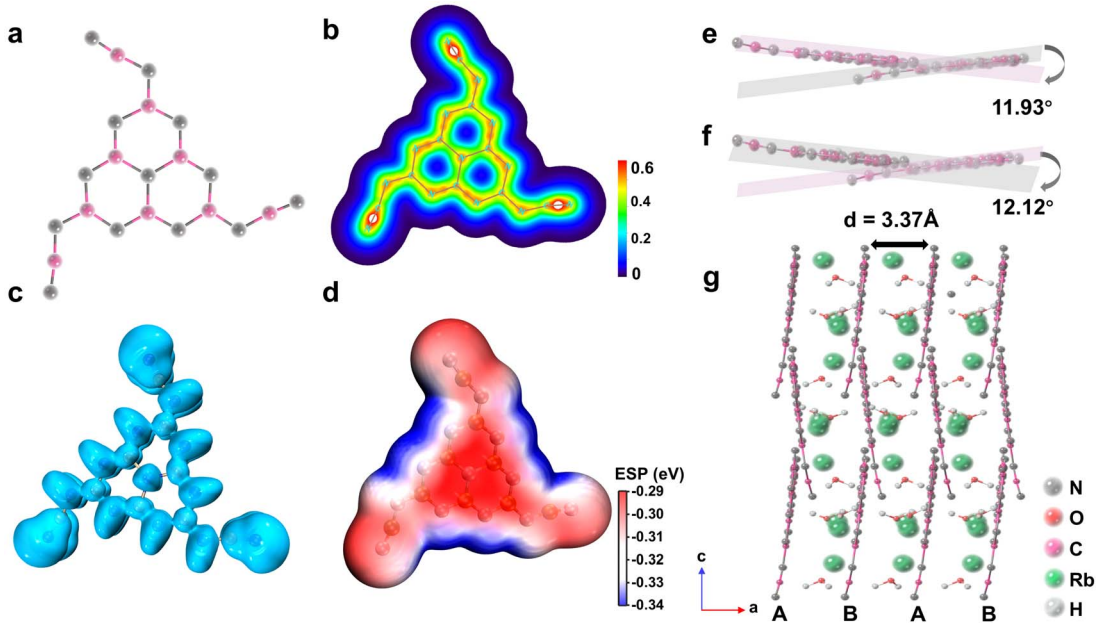

Fig. 2 (a) The planar $[C_6N_7(NCN)_3]^{3-}$ group; (b) LOL-π color-filled map of the $[C_6N_7(NCN)_3]^{3-}$ group; (c) ELF-π isosurface map of the $[C_6N_7(NCN)_3]^{3-}$ group (isovalue = 0.6); (d) the ESP of the $[C_6N_7(NCN)_3]^{3-}$ group; the inclination of the adjacent $[C_6N_7(NCN)_3]^{3-}$ groups in I (e) and II (f); (g) the 3D network structure of I consisting of multiple zig-zag $[C_6N_7(NCN)_3]_\infty$ pseudo-layers arranged in parallel along the *b*-axis.

compared to previous reports.[41,42] Both **I** and **II** crystallize in the NCS orthorhombic space group of $Pna2_1$ (no. 33). Since **I** and **II** are isostructural, the structure of **I** is described in detail as a representative. In the crystal structure of **I**, the planar $[C_6N_7(NCN)_3]^{3-}$ groups are the BBUs (Fig. 2a). The electrostatic potential (ESP) map indicates that the $[C_6N_7(NCN)_3]^{3-}$ group is non-dipole (static dipole moment μ is very close to zero), and its maximum and minimum potential regions are octupolar distributed (Fig. 2d). In the *bc*-plane, the adjacent $[C_6N_7(NCN)_3]^{3-}$ group is inclined at an angle of 11.93° (12.12° for **II**, Fig. 2e and f), forming a zig-zag $[C_6N_7(NCN)_3]_\infty$ pseudo-layer. Owing to the symmetry operations of space groups, the $[C_6N_7(NCN)_3]^{3-}$ group undergoes a vertical flip in the unit cell (Fig. S2a†), and the neighboring $[C_6N_7(NCN)_3]_\infty$ pseudo-layers also vertically flip with a torsion angle of 28.9°, resulting in the formation of two types of layers, A and B. Multiple zig-zag $[C_6N_7(NCN)_3]_\infty$ pseudo-layers are arranged parallelly in the *b*-direction following an ABAB pattern. Metal ions (Rb^+ and Cs^+) and water molecules populate the interlayers, creating the 3D network structure by ionic and hydrogen bonding, respectively (Fig. 2g). The distances between the pseudo-layers are 3.37 Å for **I**, and 3.72 Å for **II**.

The purity of the **I** and **II** polycrystalline samples was verified by powder X-ray diffraction (Fig. S3†). Needle crystals of **I** and **II** are displayed in Fig. S4a and b.† The compounds were analyzed using energy dispersive X-ray analysis and uniform distribution of elements was detected according to the elemental mapping images (Fig. S4c and d†). In addition, X-ray photoelectron spectroscopy was used to examine the chemical composition of **I** and **II** (Fig. S5 and S6†), and individual elements were identified in both compounds. The infrared spectra of **I** and **II** further confirmed the typical absorption of $[C_6N_7(NCN)_3]^{3-}$ groups (Fig. S7†).[42,43] **I** and **II** maintain good thermal stability up to 350 K and 370 K, respectively (Fig. S8†). Based on the ultraviolet-visible diffuse reflectance spectra, the UV cut-off edge of the two compounds was 325 nm, and the experimental band gaps were 3.24 and 3.20 eV, respectively (Fig. S9†). The crystals of **I** and **II** are colorless and could be used in the vis-UV range.

The second-order nonlinearity of **I** and **II** was evaluated by the Kurtz–Perry powder SHG method,[44] using a 1064 nm Q-switched Nd:YAG solid-state laser. BBO and KDP powder samples with the same particle size were used as the references. The test results show that the SHG intensity of **I** is about 1.50× BBO (9.0× KDP) within the 200–250 μm particle size range, and the value is about 1.40× BBO (8.7× KDP) for **II** (Fig. 3a). It can be seen that the SHG response increases with increasing particle size for both compounds (Fig. 3b), which are type I phase matchable and suitable for UV NLO applications. **I** and **II** have a stronger SHG response than other UV NLO materials with π-conjugation groups, including $KLi(HC_3N_3O_3)\cdot 2H_2O$ (5.1× KDP),[31] $RbNa(HC_3N_3O_3)\cdot 2H_2O$ (5.3× KDP),[45] $K_3C_6N_7O_3\cdot 2H_2O$ (4× KDP),[30] and $Cs(H_2C_3N_3S_3)$ (4.6× KDP).[46] The optical properties were calculated using the first principles theory calculation.[47] According to the Kleinman symmetry[48] of the *mm*2 point group, there are three nonzero independent SHG coefficients, and the calculated SHG coefficients for **I** are −0.38 pm V^{-1} for d_{15}, 25.16 pm V^{-1} for d_{24}, and −24.36 pm V^{-1} for d_{33}; the calculated SHG coefficients for **II** are −0.35 pm V^{-1} for d_{15}, 24.89 pm V^{-1} for d_{24}, and −24.02 pm V^{-1} for d_{33}. The calculations suggest that the experimental powder SHG of **I** and **II** could be substantially undervalued, given the fact that d_{16} of KDP is only 0.39 pm V^{-1}. The discrepancy between the powder SHG results and the calculated values may be attributed to the

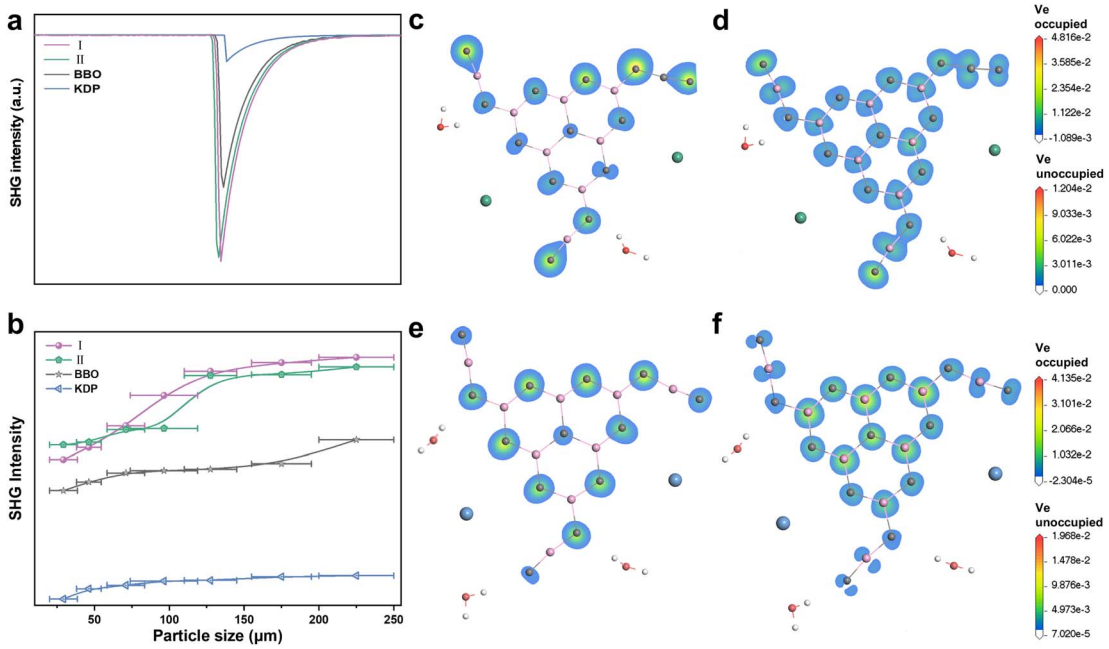

Fig. 3 (a) Oscilloscope signals showing the powder SHG intensities of I and II; (b) particle-size dependent SHG intensities of I and II; SHG-weighted electron densities for (c) occupied and (d) unoccupied electronic states in I; SHG-weighted electron densities for (e) occupied and (f) unoccupied electronic states in II.

fine-needle growth habit of **I** and **II** (see Fig. S4†), which exhibits a significant preferred orientation during the measurement process. The source of SHG for both compounds is also of interest, and the SHG-weighted electron density of the d_{z^2} orbital has been calculated. Only the virtual electron process to SHG was highlighted since it is decisive. For the occupied and unoccupied states of **I** and **II** (Fig. 3c–f), the overlap of delocalized C 2p, and N 2p orbitals is clearly visualized. In other words, the SHG-weighted electron cloud is distributed over the $[C_6N_7(NCN)_3]^{3-}$ group, whereas little SHG-weighted electron density is observed in the vicinity of the metal ions, and thus it can be stated that the compounds' SHG originates from the $[C_6N_7(NCN)_3]^{3-}$ group.

I and **II** are biaxial, and their birefringence (Δn) was measured by the interferometric color method.[49] Fig. 4a–c show the interference colors of **I** as observed under a polarizing microscope (Fig. 4d–f for **II**). The crystals appear black (complete extinction state) after the insertion of an appropriately tilted compensator (Fig. 4b and e). To improve the visibility of the extinction state, a 546 nm filter was used to remove the background color light (Fig. 4c and f). The accuracy of birefringence measurements was further verified by tilting the compensator in the opposite direction (Fig. S10†). The measured optical path differences are 2043.19 and 1964.21 nm, and the thickness of the crystals is 3.34 and 3.30 μm for **I** and **II**, respectively. Therefore, we could obtain the experimental birefringence values to be 0.612 and 0.595 for **I** and **II**, respectively. Fig. 4h and i show that the density functional theory (DFT) calculated refractive indices of **I** and **II** are $n_y > n_z > n_x$. According to the calculation results, the theoretical birefringence of **I** and **II** is 0.619@546 nm and 0.589@546 nm, respectively (Fig. 4g), which are very close to the experimental values. Such large birefringences of **I** and **II** are much larger than those of typical birefringent materials ($\Delta n < 0.3$ in UV and visible regions, *e.g.* α-BaB_2O_4, $CaCO_3$, YVO_4, and TiO_2), and are superior to those of many π-conjugated optical materials including $Cs_3C_6N_9 \cdot H_2O$ (0.520@550 nm),[29] $K_3C_6N_7O_3 \cdot 2H_2O$ (0.446@1064 nm),[30] $GU(H_2C_3N_3O_3)$ (0.419@400 nm),[50] and $Cs_2Mg(H_2C_3N_3S_3)_4 \cdot 8H_2O$ (0.580@800 nm).[51] To reveal the mechanisms and origin of significant anisotropic optical properties, the components of polarizability tensors were calculated. The α_{zz} perpendicular to the ring plane direction is 108 a.u., while the α_{xx} and α_{yy} are as high as 365 a.u. and 354 a.u. parallel to the ring plane directions. Intuitively, the polarizability anisotropy of the $[C_6N_7(NCN)_3]^3$ group is derived from the unit sphere representation maps[52] of the polarizability tensor (Fig. 4j). This illustration demonstrates how the external electric field influences the changes in dipole moment of the $[C_6N_7(NCN)_3]^{3-}$ group, *i.e.*, the induced dipole moment. The large color arrows in the center indicate projected total polarizability among *XYZ* directions. It is very clear that the polarizability attains a maximum magnitude parallel to the $[C_6N_7(NCN)_3]^{3-}$ ring plane, and is much larger than that perpendicular to the plane. Since the $[C_6N_7(NCN)_3]^{3-}$ group has extensive delocalized π electrons over C and N atoms, the addition of an external electric field parallel to the system is bound to strongly polarize the π electron distribution, resulting in a significant induced dipole moment. Since the $[C_6N_7(NCN)_3]^{3-}$ groups of **I** are more coplanar in the lattice than those of **II** (Fig. 2e and f), there is a more pronounced difference in optical anisotropy parallel and

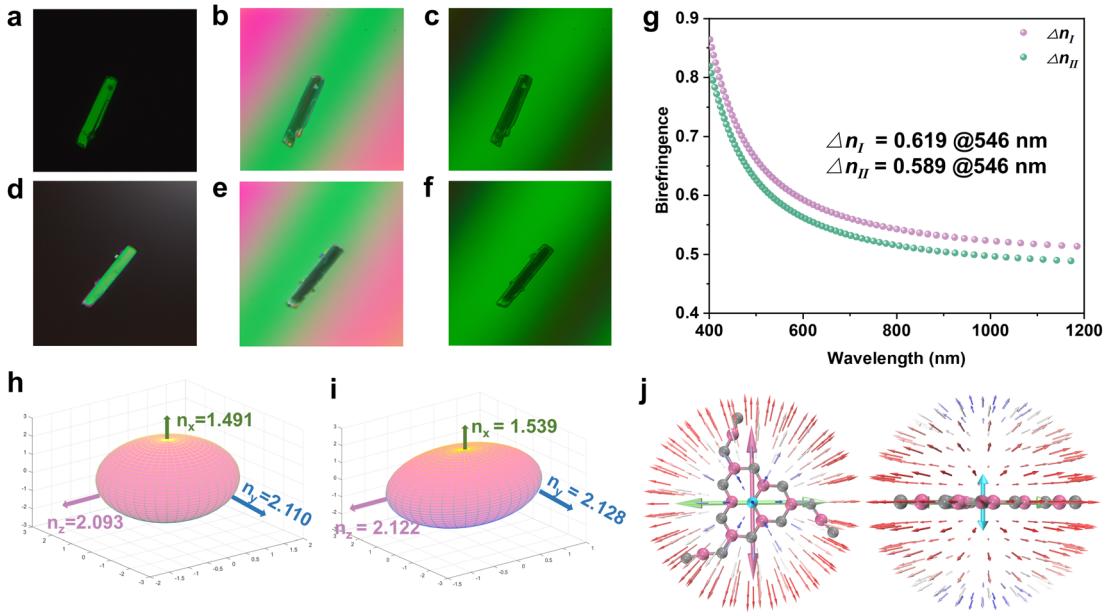

Fig. 4 (a) The interference colors of I under cross-polarized light; (b) the complete extinction of I after the insertion of the left-rotated compensator and (c) under a 546 nm monochromatic light source; (d) the interference colors of II under a polarizing microscope; (e) the complete extinction of II with the left-rotated compensator and (f) using a 546 nm filter; (g) the theoretical birefringence of I and II; (h) the refractive index of I and (i) II at 546 nm; (j) the unit sphere representation of the polarizability tensor of the octupolar $[C_6N_7(NCN)_3]^{3-}$ group. The small arrows distributed on the surface of the sphere reflect the change in the dipole moment due to the application of an external electric field of the same strength from the center, outward, in all directions. The large pink, green, and cyan arrows indicate the total magnitude of the polarizability in the *x*, *y*, and *z* directions (α_x, α_y, and α_z), respectively, which are calculated using the following equations: $\alpha_x = \alpha_{xx} + \alpha_{xy} + \alpha_{xz}$, $\alpha_y = \alpha_{yx} + \alpha_{yy} + \alpha_{yz}$, and $\alpha_z = \alpha_{zx} + \alpha_{zy} + \alpha_{zz}$.

perpendicular to the $[C_6N_7(NCN)_3]^{3-}$ groups, leading to large optical anisotropy in **I**. Moreover, statistics for compounds containing octupolar π-conjugated structures (Table S7†) show that maximum birefringence is achieved by **I** in NCS crystals (Fig. S11†).

In order to further analyze the relationship between the performance and the structure, the energy band structure is also calculated and the calculated indirect band gaps by using the GGA method are 3.09 and 3.10 eV, respectively (Fig. S12a and b†), And the calculated band gaps by using the HSE06 algorithm are 4.15 eV and 4.14 eV for **I** and **II**, respectively, which are close to the experimental band gaps. Based on the density of states (DOS) and partial density of states (PDOS) of **I** and **II**, it can be seen that N-2p orbitals mainly contribute to the top of the valence band, and C-2p orbitals occupy the bottom of the conduction band (Fig. S13a and b†). This suggests that electrons of C and N atoms show strong hybridization near the Fermi level. Since electronic transitions near the Fermi level are closely related to both linear and NLO properties, the excellent optical properties of **I** and **II** are determined by the $[C_6N_7(NCN)_3]^{3-}$ group, while the contribution from cations and water molecules is negligible.

Conclusions

In conclusion, an extended octupolar π-conjugation strategy was proposed to design advance optical materials with large SHG and birefringence. This strategy has been proved by both theoretical analysis and experimental results. Two materials with excellent optical properties- $M_3[C_6N_7(NCN)_3]\cdot 3H_2O$ (M = Rb and Cs), have been obtained by two different synthesis methods. The near coplanar $[C_6N_7(NCN)_3]^{3-}$ BBUs make these two materials exhibit a strong SHG response (~9× KDP) and a large experimental birefringence of 0.612@546 nm (for the Rb analogue), which is a record in reported organic–inorganic hybrid materials with a simultaneous optimized SHG response and birefringence. In addition, the DFT calculations confirmed that the excellent linearity and nonlinearity are due to the octupolar $[C_6N_7(NCN)_3]^{3-}$ group. We expect that the multipolar structures, especially the extended octupolar π-conjugated groups without permanent dipole moments will be an alternative system for designing new emerging photonic devices.

Data availability

The data supporting this article have been included as part of the ESI.† Crystallographic data for **I** and **II** have been deposited at the CCDC under 2375217 and 2375218.

Author contributions

The manuscript was written through contributions of all authors. Conceptualization, Y. W.; methodology, D. D.; software, D. D. and B. Z.; validation, Y. W.; formal analysis, D. D.

and Y. W.; investigation, D. D.; resources, D. Y., Y. W. and B. Z.; data curation, D. D.; writing-original draft preparation, D. D.; writing review & editing, Y. W.; visualization, D. D.; supervision, Y. W.; project administration, Y. W.; funding acquisition, Y. W. All authors have given approval to the final version of the manuscript.

Conflicts of interest

There are no conflicts to declare.

Acknowledgements

This work was supported by the National Natural Science Foundation of China (21975062, 52072109, and 22101069), the Natural Science Foundation of Hebei Province (E2023201017 and B2023201108), the Key Laboratory of Chemical Biology of Hebei Province (22567635H), and the Excellent Youth Research Innovation Team of Hebei University (QNTD202403).

Notes and references

1 Y. Zhou, Z. F. Guo, H. G. Gu, Y. Q. Li, Y. P. Song, S. Y. Liu, M. C. Hong, S. G. Zhao and J. H. Luo, A solution-processable natural crystal with giant optical anisotropy for efficient manipulation of light polarization, *Nat. Photonics*, 2024, **18**, 922–927.

2 T. T. Tran, J. Young, J. M. Rondinelli and P. S. Halasyamani, Mixed-metal carbonate fluorides as deep-ultraviolet nonlinear optical materials, *J. Am. Chem. Soc.*, 2017, **139**, 1285–1295.

3 M. Mutailipu, J. Han, Z. Li, F. M. Li, J. J. Li, F. F. Zhang, X. F. Long, Z. H. Yang and S. L. Pan, Achieving the full-wavelength phase-matching for efficient nonlinear optical frequency conversion in $C(NH_2)_3BF_4$, *Nat. Photonics*, 2023, **17**, 694–701.

4 S. F. Li, W. M. Li, X. Li, G. S. Yang, N. Ye, Z. G. Hu, Y. C. Wu and C. G. Li, A bifunctional primitive strategy induces enhancements of large second harmonic generation and wide UV transmittance in rare-earth borates containing $[B_5O_{10}]$ groups, *Chem. Sci.*, 2024, **15**, 8959–8965.

5 R. Y. Zhao, T. Zhu, S. S. Wang, C. Jarrett-Wilkins, A. M. Najjarian, A. J. Lough, S. Hoogland, E. H. Sargent and D. S. Seferos, Engineering hydrogen bonding to align molecular dipoles in organic solids for efficient second harmonic generation, *Chem. Sci.*, 2022, **13**, 12144–12148.

6 J. C. Hancock, M. L. Nisbet, W. G. Zhang, P. S. Halasyamani and K. R. Poeppelmeier, Periodic tendril perversion and helices in the $AMoO_2F_3$ (A = K, Rb, NH_4, Tl) family, *J. Am. Chem. Soc.*, 2020, **142**, 6375–6380.

7 Z. T. Yan, J. B. Fan, S. L. Pan and M. Zhang, Recent advances in rational structure design for nonlinear optical crystals: leveraging advantageous templates, *Chem. Soc. Rev.*, 2024, **53**, 6568–6599.

8 S. Bai, D. Wang, H. K. Liu and Y. Wang, Recent advances of oxyfluorides for nonlinear optical applications, *Inorg. Chem. Front.*, 2021, **8**, 1637–1654.

9 J. H. Wu, C. L. Hu, Y. F. Li, J. G. Mao and F. Kong, $[(C_5H_6N_2)_2H](Sb_4F_{13})$: a polyfluoroantimonite with a strong second harmonic generation effect, *Chem. Sci.*, 2024, **15**, 8071–8079.

10 S. De, D. Asthana, C. Thirmal, S. K. Keshri, R. K. Ghosh, G. Hundal, R. Kumar, S. Singh, R. Chatterjee and P. Mukhopadhyay, A folded π-system with supramolecularly oriented dipoles: single-component piezoelectric relaxor with NLO activity, *Chem. Sci.*, 2023, **14**, 2547–2552.

11 B. B. Zhang, G. Q. Shi, Z. H. Yang, F. F. Zhang and S. L. Pan, Fluorooxoborates: beryllium-free deep-ultraviolet nonlinear optical materials without layered growth, *Angew. Chem., Int. Ed.*, 2017, **56**, 3916–3919.

12 X. Hao, M. Luo, C. S. Lin, G. Peng, F. Xu and N. Ye, $M(NH_2SO_3)_2$ (M = Sr, Ba): two deep-ultraviolet transparent sulfamates exhibiting strong second harmonic generation responses and moderate birefringence, *Angew. Chem., Int. Ed.*, 2021, **60**, 7621–7625.

13 X. F. Wang, X. D. Leng, Y. Kuk, J. Lee, Q. Jing and K. M. Ok, Deep-ultraviolet transparent mixed metal sulfamates with enhanced nonlinear optical properties and birefringence, *Angew. Chem., Int. Ed.*, 2024, **63**, e202315434.

14 L. Xiong, J. Chen, J. Lu, C. Y. Pan and L. M. Wu, Monofluorophosphates: a new source of deep-ultraviolet nonlinear optical materials, *Chem. Mater.*, 2018, **30**, 7823–7830.

15 L. L. Wu, H. T. Tian, C. S. Lin, X. Zhao, H. X. Fan, P. X. Dong, S. D. Yang, N. Ye and M. Luo, Optimized arrangement of non-π-conjugated PO_3NH_3 units leads to enhanced ultraviolet optical nonlinearity in $NaPO_3NH_3$, *Inorg. Chem. Front.*, 2024, **11**, 1145–1152.

16 J. H. Wu, C. L. Hu, T. K. Jiang, J. G. Mao and F. Kong, Highly birefringent d^0 transition metal fluoroantimonite in the mid infrared band: order–disorder regulation by cationic size, *J. Am. Chem. Soc.*, 2023, **145**, 24416–24424.

17 L. Qi, X. X. Jiang, K. N. Duanmu, C. Wu, Z. S. Lin, Z. P. Huang, M. G. Humphrey and C. Zhang, Record second-harmonic generation and birefringence in an ultraviolet antimonate by bond engineering, *J. Am. Chem. Soc.*, 2024, **146**, 9975–9983.

18 H. P. Wu, Z. J. Wei, Z. G. Hu, J. Y. Wang, Y. C. Wu and H. W. Yu, Assembly of π-conjugated $[B_3O_6]$ units by mer-isomer $[YO_3F_3]$ octahedra to design a UV nonlinear optical material, $Cs_2YB_3O_6F_2$, *Angew. Chem., Int. Ed.*, 2024, **63**, e202406318.

19 X. H. Dong, L. Huang, C. F. Hu, H. M. Zeng, Z. E. Lin, X. Wang, K. M. Ok and G. H. Zou, $CsSbF_2SO_4$: an excellent ultraviolet nonlinear optical sulfate with a $KTiOPO_4$ (KTP)-type structure, *Angew. Chem., Int. Ed.*, 2019, **58**, 6528–6534.

20 M. Yan, C. L. Hu, R. L. Tang, W. D. Yao, W. L. Liu and S. P. Guo, $KBa_3M_2F_{14}Cl$ (M = Zr, Hf): novel short-wavelength mixed metal halides with the largest second-harmonic generation responses contributed by mixed functional moieties, *Chem. Sci.*, 2024, **15**, 8500–8505.

21 J. H. Wang, X. Y. Zhang, F. Liang, Z. G. Hu and Y. C. Wu, Co-crystal $AX\cdot(H_3C_3N_3O_3)$ (A = Na, Rb, Cs; X = Br, I): a series of strongly anisotropic alkali halide cyanurates with a planar structural motif and large birefringence, *Dalton Trans.*, 2021, **50**, 11555–11561.

22 M. Mutailipu, K. R. Poeppelmeier and S. L. Pan, Borates: a rich source for optical materials, *Chem. Rev.*, 2020, **121**, 1130–1202.

23 C. T. Chen, G. L. Wang, X. Y. Wang and Z. Y. Xu, Deep-UV nonlinear optical crystal $KBe_2BO_3F_2$—discovery, growth, optical properties and applications, *Appl. Phys. B*, 2009, **97**, 9–25.

24 C. T. Chen, Y. B. Wang, B. C. Wu, K. C. Wu, W. L. Zeng and L. H. Yu, Design and synthesis of an ultraviolet-transparent nonlinear optical crystal $Sr_2Be_2B_2O_7$, *Nature*, 1995, **373**, 322–324.

25 C. T. Chen, B. C. Wu, A. D. Jiang and G. M. You, A new-type ultraviolet SHG crystal—β-BaB_2O_4, *Sci. Sin., Ser. B*, 1985, **28**, 235–243.

26 X. H. Meng, W. L. Yin and M. J. Xia, Cyanurates consisting of intrinsic planar π-conjugated 6-membered rings: an emerging source of optical functional materials, *Coord. Chem. Rev.*, 2021, **439**, 213916.

27 M. Kalmutzki, M. Ströbele, F. Wackenhut, A. J. Meixner and H. J. Meyer, Synthesis, structure, and frequency-doubling effect of calcium cyanurate, *Angew. Chem., Int. Ed.*, 2014, **53**, 14260–14263.

28 M. J. Kalmutzki, K. Dolabdjian, N. Wichtner, M. Ströbele, C. Berthold and H. J. Meyer, Formation, structure, and frequency-doubling effect of a modification of strontium cyanurate (α-SCY), *Inorg. Chem.*, 2017, **56**, 3357–3362.

29 Y. Q. Li, Q. C. Wu, Z. S. Lin, Y. C. Liu, Y. Zhou, X. Chen, M. J. Li, M. C. Hong, J. H. Luo and S. G. Zhao, Maximizing the linear and nonlinear optical responses of alkaline tricyanomelaminate, *Fundam. Res.*, 2023, **3**, 974–978.

30 X. Y. Zhang, X. G. Du, J. H. Wang, F. Y. Wang, F. Liang, Z. G. Hu, Z. S. Lin and Y. C. Wu, $K_3C_6N_7O_3\cdot2H_2O$: a multifunctional nonlinear optical cyamelurate crystal with colossal π-conjugated orbitals, *ACS Appl. Mater. Interfaces*, 2022, **14**, 53074–53080.

31 D. H. Lin, M. Luo, C. S. Lin, F. Xu and N. Ye, $KLi(HC_3N_3O_3)\cdot2H_2O$: solvent-drop grinding method toward the hydro-isocyanurate nonlinear optical crystal, *J. Am. Chem. Soc.*, 2019, **141**, 3390–3394.

32 J. Lu, Y. K. Lian, L. Xiong, Q. R. Wu, M. Zhao, K. X. Shi, L. Chen and L. M. Wu, How to maximize birefringence and nonlinearity of pi-conjugated cyanurates, *J. Am. Chem. Soc.*, 2019, **141**, 16151–16159.

33 J. Zyss and I. Ledoux, Nonlinear optics in multipolar media theory and experiments, *Chem. Rev.*, 1994, **94**, 77–105.

34 C. Dhenaut, I. Ledoux, I. D. W. Samuel, J. Zyss, M. Bourgault and H. L. Bozec, Chiral metal complexes with large octupolar optical nonlinearities, *Nature*, 1995, **374**, 339–342.

35 Y. Liu, G. Li, X. Li and Y. Cui, Cation-dependent nonlinear optical behavior in an octupolar 3D anionic metal-organic open framework, *Angew. Chem., Int. Ed.*, 2007, **46**, 6301–6304.

36 R. Medishetty, J. K. Zaręba, D. Mayer, M. Samoć and R. A. Fischer, Nonlinear optical properties, upconversion and lasing in metal–organic frameworks, *Chem. Soc. Rev.*, 2017, **46**, 4976–5004.

37 S. Brasselet, F. Cherioux, P. Audebert and J. Zyss, New octupolar star-shaped structures for quadratic nonlinear optics, *Chem. Mater.*, 1999, **11**, 1915–1920.

38 L. Xiong, L. M. Wu and L. Chen, A general principle for DUV NLO materials: π-conjugated confinement enlarges band gap, *Angew. Chem., Int. Ed.*, 2021, **60**, 25063–25067.

39 T. Lu and Q. X. Chen, A simple method of identifying π orbitals for non-planar systems and a protocol of studying π electronic structure, *Theor. Chem. Acc.*, 2020, **139**, 25.

40 T. Lu and F. W. Chen, Multiwfn: a multifunctional wavefunction analyzer, *J. Comput. Chem.*, 2012, **33**, 580–592.

41 E. H. Bordon, E. Kroke, I. Svoboda, H. Fuess and R. Riedel, Potassium melonate, $K_3[C_6N_7(NCN)_3]\cdot5H_2O$, and its potential use for the synthesis of graphite-like C_3N_4 materials, *New J. Chem.*, 2005, **29**, 693–699.

42 S. J. Makowski and W. Schnick, $Rb_3[C_6N_7(NCN)_3]\cdot3H_2O$ and $Cs_3[C_6N_7(NCN)_3]\cdot3H_2O$ – synthesis, crystal structure and thermal behavior of two novel alkali melonates, *Z. Anorg. Allg. Chem.*, 2009, **635**, 2197–2202.

43 B. Jürgens, E. Irran, J. Senker, P. Kroll, H. Müller and W. Schnick, Melem (2,5,8-triamino-tri-*s*-triazine), an important intermediate during condensation of melamine rings to graphitic carbon nitride: synthesis, structure determination by X-ray powder diffractometry, solid-state NMR, and theoretical studies, *J. Am. Chem. Soc.*, 2003, **125**, 10288–10300.

44 S. K. Kurtz and T. T. Perry, A powder technique for the evaluation of nonlinear optical materials, *J. Appl. Phys.*, 1968, **39**, 3798–3813.

45 Y. X. Song, D. H. Lin, M. Luo, C. S. Lin, Q. L. Chen and N. Ye, $RbNa(HC_3N_3O_3)\cdot2H_2O$ exhibiting a strong second harmonic generation response and large birefringence as a new potential UV nonlinear optical material, *Inorg. Chem. Front.*, 2020, **7**, 150–156.

46 X. Hao, C. S. Lin, N. Ye, D. H. Lin, D. Zhao, Y. Q. Zhou, E. Shangguan and M. Luo, Explorations of second-order nonlinear optical materials in the monovalent trithiocyanurate system, *Cryst. Growth Des.*, 2022, **23**, 362–368.

47 M. D. Segall, J. D. L. Philip, M. J. Probert, C. J. Pickard, P. J. Hasnip, S. J. Clark and M. C. Payne, First-principles simulation: ideas, illustrations and the CASTEP code, *J. Phys. Condens. Matter*, 2002, **14**, 2717.

48 C. A. Dailey, B. J. Burke and G. J. Simpson, The general failure of Kleinman symmetry in practical nonlinear optical applications, *Chem. Phys. Lett.*, 2004, **390**, 8–13.

49 Q. Shi, L. Y. Dong and Y. Wang, Evaluating refractive index and birefringence of nonlinear optical crystals: classical methods and new developments, *Chin. J. Struct. Chem.*, 2023, **42**, 100017.

50 X. M. Liu, L. Kang, R. X. Guo and Z. S. Lin, Two metal-free cyanurate crystals with a large optical birefringence

resulting from the combination of π-conjugated units, *Dalton Trans.*, 2021, **50**, 17495–17498.

51 X. Hao, C. S. Lin, M. Luo, Y. Q. Zhou, N. Ye and E. Shangguan, $Cs_2Mg(H_2C_3N_3S_3)_4 \cdot 8H_2O$: an excellent birefringent material with giant optical anisotropy in π-conjugated trithiocyanurate, *Inorg. Chem.*, 2023, **62**, 7611–7616.

52 Z. Y. Liu, T. Lu, A. H. Yuan, X. Wang, Q. X. Chen and X. F. Yan, Remarkable size effect on photophysical and nonlinear optical properties of all-carboatomic rings, cyclo [18]carbon and its analogues, *Chem.–Asian J.*, 2021, **16**, 2267–2271.